Available online at www.sciencedirect.com
SCIENCE DIRECT®
International Journal of Mass Spectrometry 227 (2003) 21–32
International Journal of Mass Spectrometry
www.elsevier.com/locate/ijms

Anisotropic photodissociation of vinyl chloride molecular cation in the ground and first excited electronic states

Sung Hwan Yoon[a], Joong Chul Choe[b], Myung Soo Kim[a,*]

[a] *National Creative Research Initiative Center for Control of Reaction Dynamics and School of Chemistry, Seoul National University, Seoul 151-742, South Korea*
[b] *Department of Chemistry, University of Suwon, Suwon 440-600, South Korea*

Received 25 September 2002; accepted 24 October 2002

This paper is dedicated to Prof. Robert C. Dunbar on his 60th birthday.

Abstract

Photodissociation of the vinyl chloride molecular ion generated by charge exchange or electron impact ionization has been investigated using mass-analyzed ion kinetic energy spectrometry (MIKES). The MIKE spectra for the Cl and HCl losses from the vinyl chloride ion have been measured at 357, 488.0, and 514.5 nm using 0 and 90° laser polarization angles. The anisotropy parameters and kinetic energy release distributions have been determined. The vinyl chloride ion in the ground state did not undergo photodissociation in the visible spectral region while the same ion generated by more energetic means displayed fairly strong photodissociation. Presence of the vinyl chloride ion in the very long-lived first excited electronic state reported previously is compatible with this observation. In addition, isotropic dissociation to $C_2H_2^{\bullet+}$ occurring in the ground electronic state was observed. Results from the photoelectron spectroscopy and quantum chemical calculations at the TDDFT/UB3LYP/6-311++G** level were used to identify the reaction pathways involved.

Keywords: Photodissociation; Vinyl chloride ion; Long-lived excited state; MIKE spectrometry

1. Introduction

Probing excited electronic states and studying their role in chemical reactions are important research subjects in chemistry. For example, accurate calculation of excited state properties is one of the major goals in quantum chemistry [1–3]. Experimental observation of the excited electronic states and measurement of their properties are rather difficult tasks. Experimental study of the excited electronic states of polyatomic cations is more difficult than that of neutrals, one of the reasons being difficulty in preparing sufficient amount of cations. Photoionization [4,5], photoelectron spectroscopy [6–8], and photoelectron–photoion coincidence spectrometry [9–11] have been the major tools which have been used in the study of the excited electronic states. Photodissociation is also a useful technique in the study of excited state properties [12–15]. Accurate recombination energy and vibrational frequencies can often be measured by the zero electron kinetic energy spectroscopy [16–19] or mass-analyzed threshold ionization spectrometry [20–23].

* Corresponding author. Tel.: +82-2-880-6652; fax: +82-2-889-1568.
E-mail address: myungsoo@plaza.snu.ac.kr (M.S. Kim).

1387-3806/03/$ – see front matter © 2003 Elsevier Science B.V. All rights reserved.
doi:10.1016/S1387-3806(03)00051-4

Recently, we observed photodissociation of benzene molecular cation in the visible spectral region (1.8–3.1 eV) [24] even though the critical energy for dissociation is 3.66 eV [25] or larger. Careful analysis of the rate–energy data and charge exchange ionization experiment in the ion source showed that the $\tilde{A}^2E_{2g}$ state of the benzene cation, which is very long-lived, was responsible for the observed photodissociation signal. Subsequently, a technique was developed to find long-lived excited electronic states of polyatomic cations [26–28], which is based on observation of signals of charge exchange ionization occurring in a separate collision cell. In addition to the $\tilde{A}^2E_{2g}$ state of benzene cation, several long-lived states have been found, which include the $\tilde{B}^2B_2$ states of some monosubstituted benzene cations ($C_6H_5X^{\bullet+}$, X = Cl, Br, CN, and C≡CH) [27] and the $\tilde{A}^2A'$ states of some monosubstituted ethene cations ($C_2H_3X^{\bullet+}$, X = Cl, Br, I, and CN) [28]. Presence of a very long-lived excited electronic state in the vicinity of the ground state is expected to affect the photodissociation signals from these ions, as was the case for the benzene cation. Accordingly, photodissociation experiments have been performed for vinyl chloride cation ($C_2H_3Cl^{\bullet+}$). Results from the investigation are reported in this paper.

2. Experimental

A double focusing mass spectrometer with reversed geometry (VG Analytical ZAB-E) modified for photodissociation (PD) study was used in this work, Fig. 1.

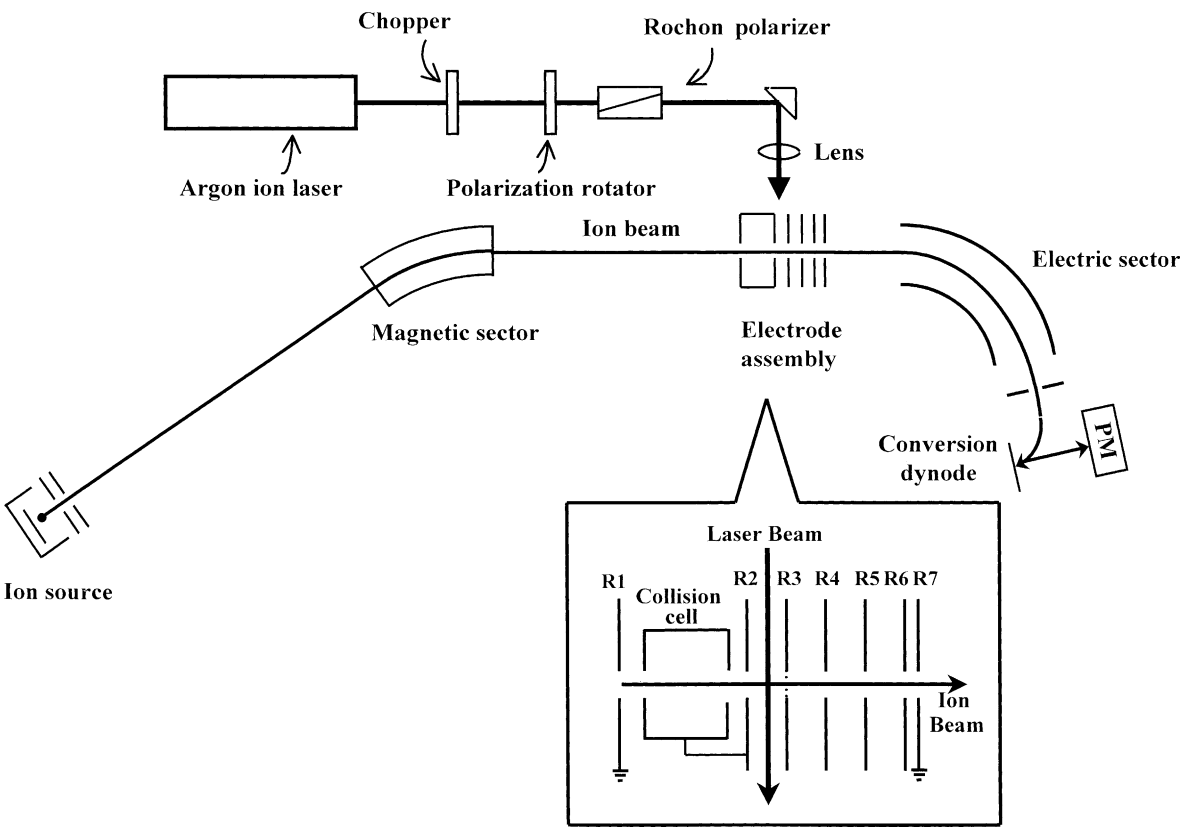

Fig. 1. Schematic diagram of the double focusing mass spectrometer with reversed geometry (VG Analytical ZAB-E) modified for photodissociation study. The inset shows the details of the electrode assembly.

Details of the modifications made were reported previously [29,30]. Vinyl chloride was introduced into the ion source via a septum inlet and ionized by electron impact ionization (EI) or charge exchange ionization (CE). CS_2 or Xe was used as a reagent gas for charge exchange ionization. Electron energy of 70 or 20 eV was used for EI or CE, respectively. Vinyl chloride ions generated in the source maintained at 140 °C were accelerated to 8 keV and $C_2H_3{}^{35}Cl^{\bullet+}$ was selected by the magnetic sector. Then, the molecular ion beam was crossed perpendicularly with a laser beam inside an electrode assembly located near the intermediate focal point of the instrument. The 514.5 and 488.0 nm lines of a Spectra Physics 164-09 argon ion laser and the 476.5 nm line and the UV-multiple lines with mean wavelength of 357 nm of a Spectra-Physics BeamLok 2065-7S argon ion laser were used for PD of the molecular ions. To measure the polarization dependence of PD, the laser polarization was rotated using a polarization rotator/rochon polarizer assembly. The translational kinetic energy of a product ion was analyzed by the electric sector. Recording the kinetic energy of product ions generated in the dissociation of mass-analyzed precursor ions is called the mass-analyzed ion kinetic energy spectrometry (MIKES) [31]. A rough estimate of the PD cross section was made by comparing with the PD yield of the *n*-butylbenzene ion measured under the same experimental condition and using the PD cross section of the latter in the literature [13,32]. A MIKE spectrum for PD, or a PD-MIKE spectrum, is often contaminated by contributions from the same reactions occurring unimolecularly (metastable ion decomposition) or by collision of the precursor ions with the residual gas. Hence, phase-sensitive detection was adopted to record a MIKE spectrum originating only from PD. Contamination by the above signals could be further reduced by recording the PD-MIKE spectra with the electrode R2 in Fig. 1 floated at a high voltage (2 kV) and the remaining electrodes of the electrode assembly grounded. To improve the quality of PD-MIKE spectra, signal averaging was carried out for repetitive scans. Errors quoted in this work were estimated from several duplicate experiments at the 95% confidence limit. All the chemicals used in this work were of the best grade commercially available.

3. Results and discussion

As has been mentioned earlier, $C_2H_3Cl^{\bullet+}$ in the ground state $\tilde{X}^2A''$ and in the long-lived state $\tilde{A}^2A'$ can be present in the ion beam generated by electron or charge exchange ionization [28]. The latter state lies higher than the former by 1.659 eV [8]. Since the present photodissociation has been studied at 357–514.5 nm (3.47–2.41 eV), various excited electronic states lying near or below 5.13 eV referred to the ionic ground state can be involved. Hence, interpretation of the experimental results can be rather complicated due to the possible participation of more than one transition. We will first present the electronic states and the properties of the transitions involving these states. Experimental results and their interpretation based on the above data will be presented thereafter.

3.1. Electronic states and electric dipole transitions

In the photoelectron spectrum of C_2H_3Cl, five bands appear in the region near and below 5.13 eV referred to the ionic ground state. These correspond to the $\tilde{X}^2A''$, $\tilde{A}^2A'$, $\tilde{B}^2A''$, $\tilde{C}^2A'$, and $\tilde{D}^2A'$ electronic states of $C_2H_3Cl^{\bullet+}$. The $\tilde{A}$, $\tilde{B}$, $\tilde{C}$, and $\tilde{D}$ states lie above the $\tilde{X}$ state by 1.659, 3.13, 3.56, and 5.35 eV [8], respectively, as estimated from the vertical energies. The energy gap of 1.659 eV between the $\tilde{A}$ and $\tilde{X}$ states is the adiabatic energy difference because the band origins are well separated from other vibrational peaks in these cases. It is to be noted that a band appearing in a photoelectron spectrum corresponds to an electronic state arising from removal of an electron in an occupied orbital of the neutral, or a hole state. An electronic state with an electron elevated to an unoccupied orbital of the neutral, which will be loosely called a LUMO state here, can also be involved in photodissociation.

Quantum chemical calculation was carried out at the time-dependent density functional theory

Table 1
Properties of the transitions from the ground ($\tilde{X}$) and first excited ($\tilde{A}$) electronic states of $C_2H_3Cl^{\bullet+}$ calculated by TDDFT/UB3LYP/6-311++G**

Transition	Main character	Energy[a] (eV)	ε[b] (°)	β[c]	Oscillator strength	PE peak[d]
$\tilde{A} \leftarrow \tilde{X}$	$n(Cl_{\parallel}) \leftarrow \pi(C{=}C)$	1.76	90	−1	0.000027	1.659
$\tilde{B} \leftarrow \tilde{X}$	$n(Cl_{\perp}) \leftarrow \pi(C{=}C)$	3.71	9	1.92	0.043708	3.13
$\tilde{C} \leftarrow \tilde{X}$	$\sigma(CCl)/\pi(CH_2)^- \leftarrow \pi(C{=}C)$	3.91	90	−1	0.000131	3.56
$\tilde{D} \leftarrow \tilde{X}$	$\sigma(C{=}C) \leftarrow \pi(C{=}C)$	5.48	90	−1	0.002168	5.35
$\tilde{E} \leftarrow \tilde{X}$	$\pi^*(C{=}C) \leftarrow \pi(C{=}C)$	5.49	20	1.66	0.188782	
$\tilde{B} \leftarrow \tilde{A}$	$n(Cl_{\perp}) \leftarrow n(Cl_{\parallel})$	1.75	90	−1	0.000021	
$\tilde{C} \leftarrow \tilde{A}$	$\sigma(CCl)/\pi(CH_2)^- \leftarrow n(Cl_{\parallel})$	1.88	17	1.75	0.003441	
$\tilde{D} \leftarrow \tilde{A}$	$\sigma(C{=}C) \leftarrow n(Cl_{\parallel})$	4.05	20	1.66	0.026272	
$\tilde{E} \leftarrow \tilde{A}$	$\pi^*(C{=}C) \leftarrow n(Cl_{\parallel})$	4.73	90	−1	0.000000	

[a] Vertical energy from the ground or first excited state at equilibrium geometry.
[b] Angle between the transition moment and the C–Cl bond axis.
[c] Anisotropy parameter estimated using $\beta = 2P_2(\cos\varepsilon)$ [50].
[d] Vertical energy from the ionic ground state measured from the photoelectron spectrum in [8].

(TDDFT) level with the UB3LYP functional and the 6-311++G** basis set, TDDFT/UB3LYP/6-311++G**, using the Gaussian 98 package [33]. This was to study the properties of the low-lying electronic states and of the electric dipole transitions connecting these states and to find LUMO states which lie in the energy range investigated. Four hole states were found at 1.76, 3.71, 3.91, and 5.48 eV [33] above the ground state as listed in Table 1 which match well with those at 1.659, 3.13, 3.56, and 5.35 eV, respectively, in the photoelectron spectrum. It was also found that $\tilde{X}$, $\tilde{A}$, $\tilde{B}$, $\tilde{C}$, and $\tilde{D}$ are the states which arise by removal of an electron from π(C=C), $n(Cl_{||})$, $n(Cl_{\perp})$, $\sigma(CCl)/\pi(CH_2)^-$, and σ(C=C) orbitals of the neutral. Here $n(Cl_{||})$ and $n(Cl_{\perp})$ denote the non-bonding 3p orbitals of chlorine lying parallel and perpendicular to the molecular plane, respectively. The lowest-lying LUMO state, or the $\tilde{E}$ state, was found at 5.49 eV (vertical energy). This state arises by elevation of an electron in the π(C=C) orbital to the π^*(C=C) orbital. 5.49 eV needed for the $\tilde{E} \leftarrow \tilde{X}$ transition is larger than the most energetic photon energy (357 nm, 3.47 eV) used in this work. Namely, this state does not have to be considered for photoexcitation from the ground state. This state is not important for photoexcitation from the $\tilde{A}$ state either, because the $\tilde{E} \leftarrow \tilde{A}$ transition is a two electron process and would have a very low probability. The lowest quartet state was found at 5.70 eV above the ground state, which is the vertical energy. This state does not have to be considered either for similar reasons. We also optimized the geometry in the $\tilde{A}$ state and calculated the vertical energies from this state to the $\tilde{B}$–$\tilde{E}$ states. The results are listed in Table 1. Also listed in the table are the oscillator strengths, the angles (ε) between the transition moment and the C–Cl bond axis, and the anisotropy parameters (to be explained) for the optical transitions from the $\tilde{X}$ and $\tilde{A}$ states.

Electronically excited products can be produced by dissociation of highly excited ions. The upper spin-orbit level ($^2P_{1/2}$) of $Cl^{\bullet}$ in the ground electronic state lies 0.11 eV [34] above the lower level ($^2P_{3/2}$). This difference is too small to be detectable in the kinetic energy release distribution obtained in this work, as will be shown below. The first excited electronic states of $C_2H_3^+$ and $Cl^{\bullet}$, which are the major products generated in this work, lie 6.63 eV [33] and 8.92 eV [34] above the ground states, respectively. Hence, generation of these ions in the excited electronic states is not energetically possible.

3.2. *Photodissociation of $C_2H_3Cl^{\bullet+}$ generated by charge exchange with $CS_2^{\bullet+}$*

Charge exchange ionization by $CS_2^{\bullet+}$ has been used in this laboratory as a method to prepare

Table 2
Molecular parameters used in the calculations of thermal internal energy distribution and KERDs

Vibrational frequencies[a] (cm^{-1})	
$C_2H_3Cl^{\bullet+}$	387, 403, 823, 853, 1019, 1077, 1279, 1386, 1506, 3134, 3183, 3250
$C_2H_3^+$	447, 661, 777, 923, 1199, 1980, 2314, 3264, 3375
Rotational constants[a] (cm^{-1})	
$C_2H_3Cl^{\bullet+}$	1.81, 0.21, 0.19
$C_2H_3^+$	13.37, 1.15, 1.06
Polarizability[b] ($10^{-24}\,cm^3$)	
Cl	2.18

[a] DFT calculation at the UB3LYP/6-311++G** level.
[b] From ref. [51].

molecular ions with well-defined (±0.1 eV) internal energy [35,36] given by

$$E = \mathrm{RE} - \mathrm{IE} + E_{\mathrm{th}} \quad (1)$$

Here RE is the recombination energy of $CS_2^{\bullet+}$ which is 10.07 eV [37], IE is the ionization energy of the sample, and E_{th} is the thermal energy. The thermal energy distribution at 140 °C was calculated using the molecular parameters in Table 2. Its average was 0.11 eV. Taking 10.005 eV as IE [8], the average internal energy of $C_2H_3Cl^{\bullet+}$ becomes 0.18 eV. Namely, nearly thermal $C_2H_3Cl^{\bullet+}$ in the ground electronic state is generated by CS_2 charge exchange.

We attempted but failed to photodissociate $C_2H_3Cl^{\bullet+}$ generated by CS_2 charge exchange using several visible lines of an argon ion laser such as at 514.5, 488.0, and 476.5 nm (the upper limit of the cross sections at these wavelengths were $\sim 5 \times 10^{-20}\,cm^2$ as estimated from the noise level). This is in agreement with the fact that intensity of the $\tilde{A}$–$\tilde{X}$ transition is very weak as indicated by the very long lifetime of the $\tilde{A}$ state [28] and also by very poor oscillator strength calculated for this transition. Alternatively, dissociation may not occur even though a photon is absorbed because the internal energy of $C_2H_3Cl^{\bullet+}$ after photoabsorption is not sufficient for rapid dissociation. Rate–energy information is needed to check such a possibility. $C_2H_3^+$ and $C_2H_2^{\bullet+}$ generated by the following reactions are the fragments with the lowest appearance energy, 12.54 ± 0.02 eV [38] and 12.47 ± 0.1 eV [39], respectively.

$$C_2H_3Cl^{\bullet+} \rightarrow C_2H_3^+ + Cl^{\bullet} \quad (2)$$

$$C_2H_3Cl^{\bullet+} \rightarrow C_2H_2^{\bullet+} + HCl \quad (3)$$

With IE(C_2H_3Cl) of 10.005 eV, the critical energies for these reactions are 2.54 and 2.47 eV, respectively. In comparison, the average internal energies of $C_2H_3Cl^{\bullet+}$ after absorption of one photon at 514.5 (2.41 eV), 488.0 (2.54 eV), and 476.5 nm (2.60 eV) are 2.59, 2.72, and 2.78 eV, respectively. We estimated the rate–energy relation for reaction (2) with the Rice–Ramsperger–Kassel–Marcus theory [40] using the critical energy of 2.54 eV and the entropy of activation at 1000 K of 7.0 eu (29 J mol^{-1} K^{-1}). The rate constant was $8 \times 10^7\,s^{-1}$ at the threshold (2.54 eV) and increased rapidly to $1 \times 10^{10}\,s^{-1}$ at 2.78 eV (476.5 nm excitation). Lowering the entropy of activation to 3.0 eu (13 J mol^{-1} K^{-1}) which is unreasonably low for a simple cleavage, the threshold rate constant became $2 \times 10^7\,s^{-1}$. On the other hand, the present apparatus can detect a photodissociation signal occurring with a rate constant $10^6\,s^{-1}$ or larger. Hence, it is clear that photodissociation was not observed in the visible spectral region not because the internal energy after photoabsorption was not sufficient for rapid dissociation but because $C_2H_3Cl^{\bullet+}$ did not absorb at these wavelengths. This is in agreement with the extremely small probability for the $\tilde{A}$–$\tilde{X}$ transition postulated from the previous experimental results [28] and also found by quantum chemical calculations.

In contrast, photodissociation at 357 nm occurred efficiently (cross section: $\sim 5 \times 10^{-18}\,cm^2$) and generated $C_2H_3^+$ via reaction (2). The PD-MIKE profiles of $C_2H_3^+$ obtained with the laser polarization parallel (0°) and perpendicular (90°) to the ion beam direction are shown in Fig. 2(a). Dramatic change of the profile with the laser polarization means that the reaction proceeds very rapidly, on a time scale comparable to or faster than the rotational period of the reactant. The angular distribution of a photodissociation product is given by [41]

$$I(\Theta) = \frac{1}{4\pi}[1 + \beta P_2(\cos\Theta)] \quad (4)$$

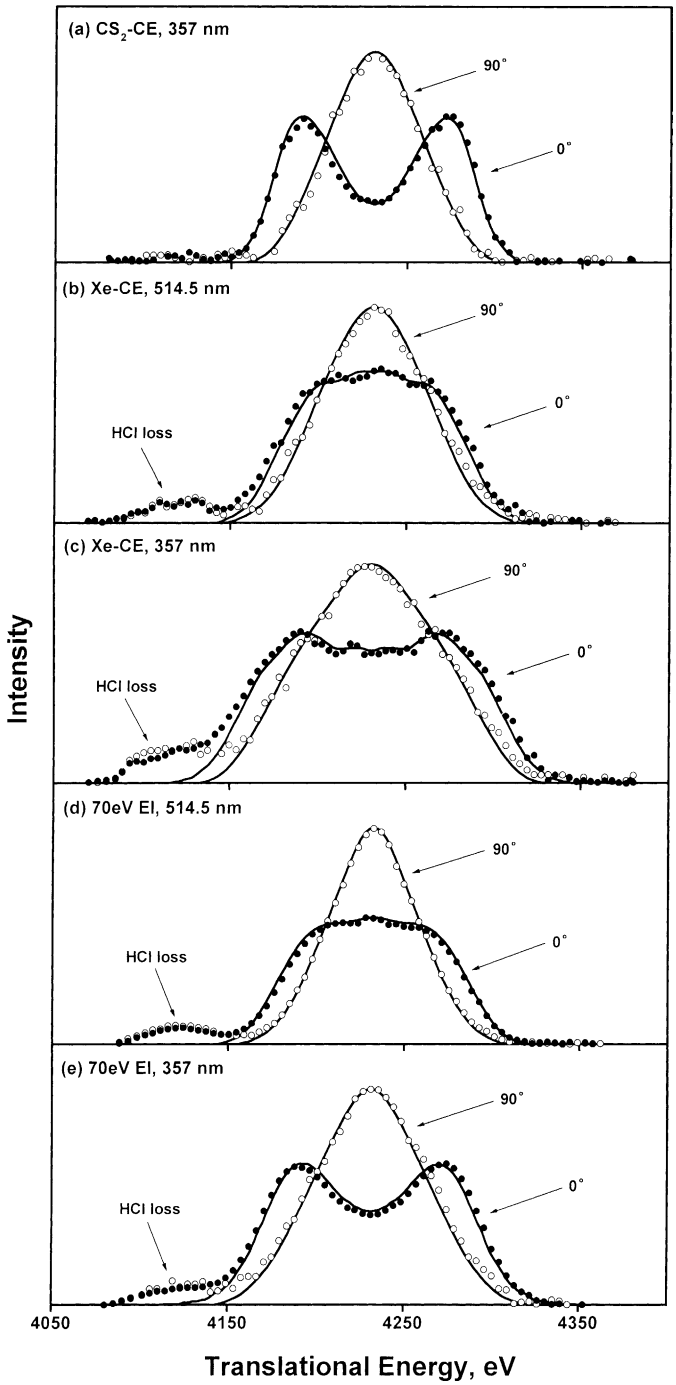

Fig. 2. PD-MIKE profiles for the Cl loss from $C_2H_3Cl^{\bullet+}$. Method to generate $C_2H_3Cl^{\bullet+}$ and photodissociation wavelength are (a) CS_2-CE and 357 nm, (b) Xe-CE and 514.5 nm, (c) Xe-CE and 357 nm, (d) 70 eV EI and 514.5 nm, and (e) 70 eV EI and 357 nm. Filled (●) and open (○) circles indicate laser polarization angle of 0 and 90°, respectively. Lines are the profiles calculated using $n(T)$ and $\beta(T)$ in Figs. 3 and 4 obtained by analyzing the experimental profiles shown here.

Here, Θ is the angle between the electric vector of the light and the product recoil direction and P_2 is the second-degree Legendre polynomial. β is the anisotropy parameter which ranges from -1 to $+2$ and characterizes the degree of dissociation anisotropy. $\beta = +2$ and -1 correspond to dissociation occurring parallel and perpendicular to the transition moment, respectively. $\beta = 0$ corresponds to an isotropic dissociation. Also, the kinetic energy profile of the product ion, or MIKE profile, is broadened due to the release of internal energy into the translational degrees of freedom of products, or kinetic energy release (KER). A numerical method to obtain distributions of KER and β, $n(T)$ and $\beta(T)$, respectively, from the experimental PD-MIKE profiles obtained at two or more polarizations was reported previously [13,14]. $n(T)$ and $\beta(T)$ obtained from PD-MIKE profiles in Fig. 2(a) are shown in Fig. 3(a). PD-MIKE profiles were calculated using these distributions to assure the reliability of data analysis. The results are compared with the experimental profiles in Fig. 2(a). The averages of KER and β, namely $\bar{T}$ and $\bar{\beta}$, calculated from these distributions are 0.38 eV and 1.5, respectively. $\bar{T}$, $\bar{\beta}$, cross section, and other pertinent data for all the photodissociation works carried out here are listed in Table 3.

Considering energetics only, two transitions, $\tilde{B} \leftarrow \tilde{X}$ and $\tilde{C} \leftarrow \tilde{X}$, can contribute to absorption at 357 nm (3.47 eV) by $C_2H_3Cl^{\bullet+}$ in the ground state. However, the latter is not likely because of the very poor oscillator strength and negative β (Table 1). Large oscillator strength and the anisotropy parameter of 1.92 calculated for the former are compatible with the experimental results. Regardless, it is not clear in which electronic state the dissociation actually occurs. Even though the $\tilde{B}$ state was found not to have a very long lifetime in our previous work [28], it would not be a repulsive state considering that it is characterized by an unpaired electron in the nonbonding $3p_\perp$ orbital of chlorine. Suppose that the $\tilde{B} \rightarrow \tilde{X}$ internal conversion occurs rapidly, within several picoseconds. Then, complete conversion of the electronic energy to the vibrational energy in the $\tilde{X}$ state assures rapid dissociation according to the statistical rate–energy relation mentioned above. A similar mechanism was proposed for anisotropic dissociation of highly excited 1-$C_3H_7I^{\bullet+}$ in our previous work [42]. An alternative explanation is based on the fact that the $\tilde{B}$ and $\tilde{C}$ bands heavily overlap in the photoelectron spectrum [6–8] and that the $\tilde{C}$ state is likely to be repulsive due to removal of an electron from the bonding σ(CCl) orbital. Namely, excitation to the $\tilde{B}$ state followed by curve crossing to the repulsive $\tilde{C}$ state can be compatible with the experimental results.

As an attempt to gain further information on the dissociation step, statistically expected kinetic energy release distribution (KERD) for reaction (2) was calculated with the phase space theory [43–46].

$$n(T; J, E) \propto \int_{R_m}^{E-E_0-T} \rho(E - E_0 - T - R) \times P(T, J, R)\, dR \quad (5)$$

Table 3
Kinetic energy releases, anisotropy parameters, cross sections, and relative abundances for reaction (2)

λ (nm)	Ionization	E_{avl}[a] (eV)	$\bar{T}$ (eV)	$\bar{\beta}$	Cross section (10^{-17} cm^2)	RA[b] (%)
357	CS_2-CE	1.11	0.38 ± 0.04	1.50 ± 0.1	0.5	>99
	Xe-CE	3.16	0.60 ± 0.08	0.94 ± 0.11	0.8	92
	EI	–	0.54 ± 0.04	1.00 ± 0.1	1	95
488.0	Xe-CE	2.23	0.41 ± 0.05	0.73 ± 0.17	0.2	94
	EI	–	0.38 ± 0.02	0.83 ± 0.07	0.2	95
514.5	Xe-CE	2.10	0.38 ± 0.04	0.69 ± 0.16	0.2	94
	EI	–	0.35 ± 0.02	0.80 ± 0.08	0.2	95

[a] Average available energy in the dissociation of the photoexcited $C_2H_3Cl^{\bullet+}$ ions to products. For charge exchange ionization, Eq. (1) was used.
[b] Relative abundance of reaction (2). The other channel is the HCl loss, reaction (3).

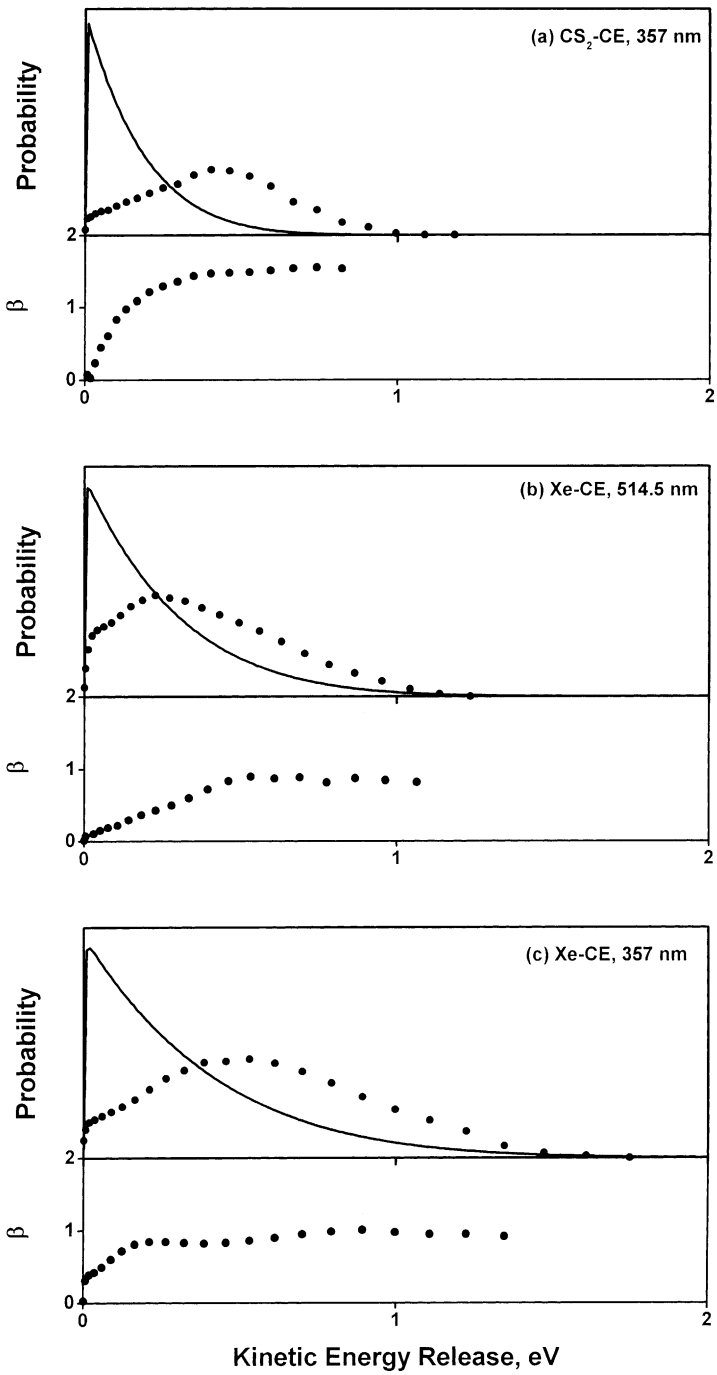

Fig. 3. Distributions of the kinetic energy release $n(T)$ and the anisotropy parameter $\beta(T)$ obtained by analyzing MIKE profiles for photodissociation of $C_2H_3Cl^{\bullet+}$ generated by charge exchange in Fig. 2. Method to generate $C_2H_3Cl^{\bullet+}$ and photodissociation wavelength are (a) CS_2-CE and 357 nm, (b) Xe-CE and 514.5 nm, and (c) Xe-CE and 357 nm. Filled circles indicate the experimental results. Lines are the statistically expected KERDs for dissociation in the ground electronic state calculated by phase space theory.

Here, $n(T; J, E)$ is the probability to release kinetic energy T for reactant with internal energy E and angular momentum J. The root-mean-square average J calculated at the ion source temperature was used. ρ and P are the product vibrational and angular momentum state densities, respectively. R is the product rotational energy, R_m is its minimum, and E_0 is the reaction critical energy. Molecular parameters used in the calculation are listed in Table 2. 2.54 eV was taken as the critical energy as mentioned before. Internal energy of $C_2H_3Cl^{\bullet+}$ was taken as the sum of the pre-excitation average energy (0.18 eV) and the photon energy (357 nm, 3.47 eV), 3.65 eV. KERD thus calculated is compared with the experimental one in Fig. 3(a). The fact that the statistically expected KER is much smaller than observed indicates that dissociation in the ground state is not the major reaction pathway. Minor irregular feature at low KER region of the experimental KERD in Fig. 3(a) may be due to contribution from the ground state dissociation. In addition to the KERD data, absence of HCl loss channel, reaction (3), in the experimental PD-MIKE spectrum is another evidence for the excited state dissociation, as will be presented later.

3.3. Photodissociation of $C_2H_3Cl^{\bullet+}$ generated by charge exchange with $Xe^{\bullet+}$

Charge exchange with a noble gas ion is also a good way of generating molecular ions with well-defined internal energy. Charge exchange with $Xe^{\bullet+}$ in the ground state (RE = 12.12 eV) [47] generates $C_2H_3Cl^{\bullet+}$ with 2.12 eV internal energy. Adding the average thermal energy of 0.11 eV, the total internal energy becomes 2.23 eV, which is below the critical energies for reactions (2) and (3). Energy transfer of 2.12 eV at the time of charge exchange is sufficient to generate $C_2H_3Cl^{\bullet+}$ in the $\tilde{A}$ state. Hence, one expects that $C_2H_3Cl^{\bullet+}$ in both $\tilde{X}$ and $\tilde{A}$ states are present in the ion beam generated by Xe charge exchange. It is known that an excited electronic state of $Xe^{\bullet+}$ with recombination energy 13.44 eV is metastable [6,48] and can contribute to ionization of C_2H_3Cl. $C_2H_3Cl^{\bullet+}$ ions thus generated would dissociate in the ion source except those generated in the $\tilde{A}$ state.

Unlike $C_2H_3Cl^{\bullet+}$ generated by CS_2 charge exchange, ions generated here displayed fairly strong photodissociation signals in the visible spectral region. The PD-MIKE profiles obtained at 514.5 nm are shown in Fig. 2(b). It is to be noted that the HCl loss channel, reaction (3), also occurs in this case. Also to be noted is that the PD-MIKE profile of $C_2H_3^+$ is polarization dependent, or anisotropic, while that of $C_2H_2^{\bullet+}$ is apparently isotropic. This indicates participation of more than one reaction channel. $n(T)$ and $\beta(T)$ were calculated by analyzing the PD-MIKE profiles. The results are shown in Fig. 3(b). $\bar{T}$ and $\bar{\beta}$ obtained from the distributions, 0.38 eV and 0.69, respectively, are listed in Table 3. The PD-MIKE profiles obtained at 488.0 nm are similar to the present data and will not be presented here, even though the results of the analysis are listed in Table 3.

We have mentioned earlier that the $\tilde{A} \leftarrow \tilde{X}$ transition is extremely unlikely. Considering that $C_2H_3Cl^{\bullet+}$ generated by Xe charge exchange possesses 2.23 eV internal energy and gains 2.41 eV more by absorption of a 514.5 nm photon, one may think that the $\tilde{B} \leftarrow \tilde{X}$ transition is involved in the photodissociation in the visible spectral region. Such a vibrationally aided photodissociation is possible only when the internal energy is concentrated in a particular vibrational mode, such as the O–H stretching mode in H_2O [49]. In more general cases, which is highly likely for the present case, internal energy is distributed among all the vibrational degrees of freedom through rapid intramolecular vibrational redistribution, resulting in each mode being mostly in its ground or first excited level. Hence, the $\tilde{B} \leftarrow \tilde{X}$ transition with ~3.13 eV transition energy is highly unlikely at 514.5 nm (2.41 eV). Then, the fact that photodissociation in the visible spectral region is observed for $C_2H_3Cl^{\bullet+}$ generated by Xe charge exchange confirms the presence of $C_2H_3Cl^{\bullet+}$ in an excited electronic state, which is the $\tilde{A}$ state according to our previous study. Considering energetics only, $\tilde{B} \leftarrow \tilde{A}$ and $\tilde{C} \leftarrow \tilde{A}$ are the transitions involved in photodissociation at 514.5 nm. Very small oscillator strength and negative anisotropy calculated for the

former, Table 1, are not compatible with the experimental results. Calculated data for the latter are in general agreement with the experimental data even though the calculated oscillator strength looks a little small. Since the $\tilde{C}$ state is likely to be repulsive, dissociation would occur directly in this state. However, curve crossing to the $\tilde{X}$ state must also occur as indicated by appearance of the HCl loss channel in the PD-MIKE spectrum.

Photodissociation at 357 nm also generated intense signals. Its MIKE profiles are shown in Fig. 2(c). $n(T)$ and $\beta(T)$ obtained by analyzing these profiles are shown in Fig. 3(c). Isotropic formation of $C_2H_2^{\bullet+}$ via HCl loss also occurs at this wavelength. $\bar{T}$ and $\bar{\beta}$ calculated from the distributions are listed in Table 3. Photodissociation at this wavelength is more complicated because excitation from both the $\tilde{X}$ and $\tilde{A}$ states are involved. For ions in the $\tilde{X}$ state, the $\tilde{B} \leftarrow \tilde{X}$ optical transition followed by the $\tilde{C} \leftarrow \tilde{B}$ internal conversion would be the main photodissociation pathway as has been suggested earlier. The $\tilde{B}$ and $\tilde{C}$ states are energetically accessible when $C_2H_3Cl^{\bullet+}$ in the $\tilde{A}$ state absorbs one photon at 357 nm (3.47 eV). As before, the $\tilde{B} \leftarrow \tilde{A}$ transition is not likely because of the poor oscillator strength while the $\tilde{C} \leftarrow \tilde{A}$ transition is feasible. Appearance of the HCl loss channel

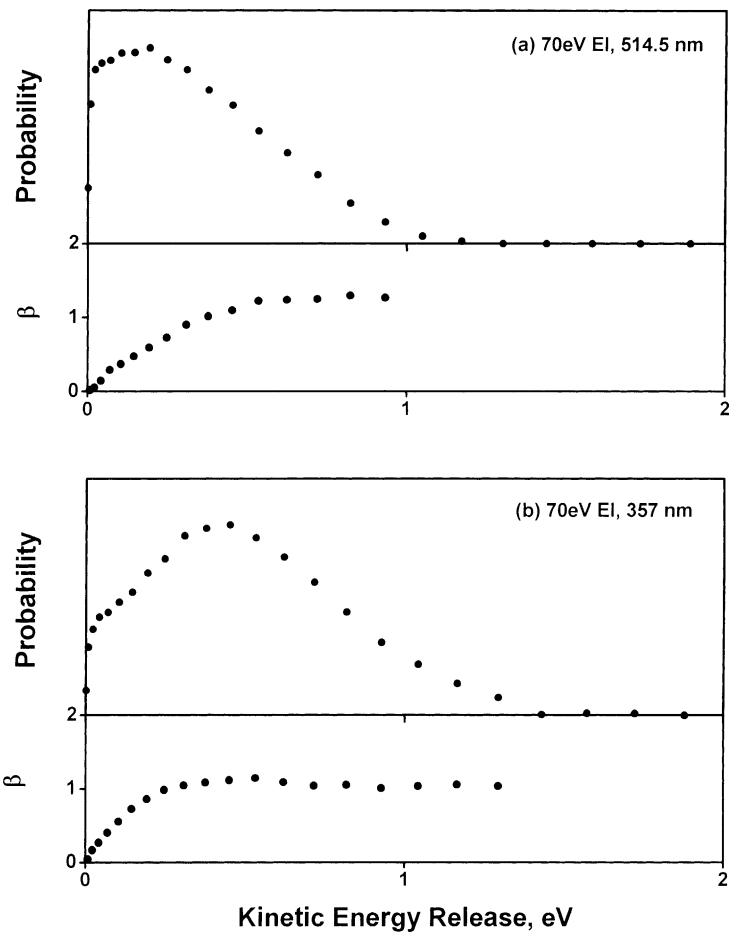

Fig. 4. Distributions of the kinetic energy release $n(T)$ and the anisotropy parameter $\beta(T)$ obtained by analyzing MIKE profiles for photodissociation of $C_2H_3Cl^{\bullet+}$ generated by 70 eV EI in Fig. 2. Photodissociation at (a) 514.5 nm and (b) 357 nm. Filled circles indicate the experimental results.

in Fig. 2(c) indicates participation of this transition in addition to the $\tilde{B} \leftarrow \tilde{X}$ transition mentioned above. We cannot judge whether the $\tilde{D} \leftarrow \tilde{A}$ transition is also involved in photodissociation at 357 nm because the energetics data available are not accurate enough.

3.4. Photodissociation of $C_2H_3Cl^{\bullet+}$ generated by 70 eV electron impact ionization

PD-MIKE profiles obtained at 514.5 and 357 nm for $C_2H_3Cl^{\bullet+}$ generated by 70 eV electron impact ionization are shown in Fig. 2(d) and (e). $n(T)$ and $\beta(T)$ obtained by analyzing these profiles are shown in Fig. 4(a) and (b). Experimental $\bar{T}$, $\bar{\beta}$, and cross section data are listed in Table 3. It is evident that photodissociation results in this case are very similar to those obtained for $C_2H_3Cl^{\bullet+}$ generated by Xe charge exchange. It is to be emphasized again that $C_2H_3Cl^{\bullet+}$ ions in the $\tilde{X}$ and $\tilde{A}$ states are present in the ion beam generated by 70 eV electron impact ionization even after ~25 μs needed for their flight from the ion source to the photodissociation site. The radiative lifetime of the $\tilde{A}$ state, 280 μs, evaluated with the oscillator strength in Table 1 is compatible with this observation. The present observation is a further evidence for the very long lifetime of $C_2H_3Cl^{\bullet+}$ in the $\tilde{A}$ state suggested in our previous work [28].

4. Summary and conclusion

Presence of a very long-lived excited electronic state of $C_2H_3Cl^{\bullet+}$ provided a rare opportunity to investigate ionic photodissociation processes in some detail. Especially useful was the selective generation of $C_2H_3Cl^{\bullet+}$ ions in the ground state, which established that visible photon was not absorbed by the ground state ion. This was in contrast with the efficient photodissociation of the same ion generated by Xe charge exchange or by 70 eV electron impact ionization, which probably occurred due to the presence of $C_2H_3Cl^{\bullet+}$ in the very long-lived first excited electronic state, $\tilde{A}^2A'$. All the photodissociation processes generating $C_2H_3^+$ were found to occur anisotropically. For $C_2H_3Cl^{\bullet+}$ in the ground state, the $\tilde{B} \leftarrow \tilde{X}$ optical transition followed by the $\tilde{C} \leftarrow \tilde{B}$ curve crossing and repulsive dissociation therein was the main reaction pathway while the $\tilde{C} \leftarrow \tilde{A}$ optical transition was responsible for photodissociation of $C_2H_3Cl^{\bullet+}$ in the $\tilde{A}$ state. Isotropic photodissociation to $C_2H_2^{\bullet+}$ was also observed in the latter case, indicating dissociation in the ground state. We cannot explain at the moment why the HCl loss channel is observed in the photodissociation of the $\tilde{A}$ state ions while it is absent in that of the $\tilde{X}$ state ions even though dissociation seems to occur in the $\tilde{C}$ state in both cases. One can only guess that the locations on the $\tilde{C}$ state potential energy surface sampled are different in the two cases. A thorough quantum chemical study of the potential energy surfaces involved would be needed to resolve this issue.

Acknowledgements

This work was supported financially by CRI, Ministry of Science and Technology, Republic of Korea. S. H. Yoon thanks the Ministry of Education for the Brain Korea 21 fellowship.

References

[1] M. Olivucci, I.N. Ragazos, F. Bernardi, M.A. Robb, J. Am. Chem. Soc. 115 (1993) 3710.
[2] J.B. Foresman, M. Head-Gordon, J.A. Pople, M.J. Frisch, J. Phys. Chem. 96 (1992) 135.
[3] M.E. Casida, C. Jamorski, K.C. Casida, D.R. Salahub, J. Chem. Phys. 108 (1998) 4439.
[4] J. Momigny, Nature 199 (1963) 1179.
[5] J. Momigny, C. Goffart, L. D'or, Int. J. Mass Spectrom. Ion Phys. 1 (1968) 53.
[6] K. Kimura, S. Katsumata, Y. Achiba, T. Yamazaki, S. Iwata, Handbook of HeI Photoelectron Spectra of Fundamental Organic Molecules, Japan Scientific Societies, Tokyo, 1981.
[7] K.H. Sze, C.E. Brion, A. Katrib, B. El-Issa, Chem. Phys. 137 (1989) 369.
[8] R. Locht, B. Leyh, K. Hottmann, H. Baumgartel, Chem. Phys. 220 (1997) 217.
[9] R.G. Orth, R.C. Dunbar, J. Chem. Phys. 68 (1978) 3254.
[10] B.E. Miller, T. Baer, Chem. Phys. 85 (1984) 39.
[11] I.C. Lane, I. Powis, J. Phys. Chem. 97 (1993) 5803.
[12] T.L. Bunn, T. Baer, J. Chem. Phys. 85 (1986) 6361.

[13] D.Y. Kim, J.C. Choe, M.S. Kim, J. Chem. Phys. 113 (2000) 1714.
[14] D.S. Won, M.S. Kim, J.C. Choe, T.K. Ha, J. Chem. Phys. 115 (2001) 5454.
[15] S.T. Park, S.K. Kim, M.S. Kim, Nature 415 (2002) 306.
[16] K. Mûller-Dethlefs, E.W. Schlag, Annu. Rev. Phys. Chem. 42 (1991) 109.
[17] T.G. Wright, S.I. Panov, T.A. Miller, J. Chem. Phys. 102 (1995) 4793.
[18] J.W. Hepburn, Chem. Soc. Rev. 25 (1996) 281.
[19] E.W. Schlag, ZEKE Spectroscopy, Cambridge University Press, Cambridge, 1998.
[20] H. Krause, H.J. Neusser, J. Chem. Phys. 97 (1992) 5923.
[21] S.T. Park, S.K. Kim, M.S. Kim, J. Chem. Phys. 114 (2001) 5568.
[22] S.T. Park, S.K. Kim, M.S. Kim, J. Chem. Phys. 115 (2001) 2492.
[23] C.H. Kwon, H.L. Kim, M.S. Kim, J. Chem. Phys. 116 (2002) 10361.
[24] M.S. Kim, C.H. Kwon, J.C. Choe, J. Chem. Phys. 113 (2000) 9532.
[25] Th.L. Grebner, H.J. Neusser, Int. J. Mass Spectrom. 185/186/187 (1999) 517.
[26] C.H. Kwon, J.C. Choe, M.S. Kim, J. Am. Soc. Mass Spectrom. 12 (2001) 1120.
[27] Y.Y. Youn, C.H. Kwon, J.C. Choe, M.S. Kim, J. Chem. Phys. 117 (2002) 2538.
[28] Y.Y. Youn, J.C. Choe, M.S. Kim, J. Am. Soc. Mass Spectrom. 14 (2003) 110.
[29] J.C. Choe, M.S. Kim, J. Phys. Chem. 95 (1991) 50.
[30] S.H. Lim, J.C. Choe, M.S. Kim, J. Phys. Chem. A 102 (1998) 7375.
[31] R.G. Cooks, J.H. Beynon, R.M. Caprioli, G.R. Lester, Metastable Ions, Elsevier, Amsterdam, 1973.
[32] J.H. Chen, J.D. Hays, R.C. Dunbar, J. Phys. Chem. 88 (1984) 4759.
[33] M.J. Frisch, G.W. Trucks, H.B. Schlegel, et al., Gaussian 98, Gaussian, Inc., Pittsburgh, PA, 1998.
[34] Gas Phase Ion Energetics, in: NIST Chemistry WebBook: NIST Standard Reference Database Number 69 [Natl. Inst. Standards and Tech. (http://webbook.nist.gov), Gaithersberg, MD, 1988].
[35] Y.H. Yim, M.S. Kim, J. Phys. Chem. 98 (1994) 5201.
[36] S.T. Oh, J.C. Choe, M.S. Kim, J. Phys. Chem. 100 (1996) 13367.
[37] S.G. Lias, J.E. Bartmess, J.F. Liebman, J.L. Holmes, R.D. Levine, W.G. Mallard, J. Phys. Chem. Ref. Data 17 (Suppl. No. 1) (1988) 77.
[38] L. Sheng, F. Qi, L. Tao, Y. Zhang, S. Yu, C. Wong, W. Li, Int. J. Mass Spectrom. Ion Processes 148 (1995) 179.
[39] D. Reinke, R. Kraessig, H. Baumgärtel, Z. Naturforsch. A 28 (1973) 1021.
[40] P.J. Robinson, K.A. Holbrook, Unimolecular Reactions, Wiley, New York, 1972.
[41] R.N. Zare, Mol. Photochem. 4 (1972) 1.
[42] S.T. Park, M.S. Kim, J. Chem. Phys. 117 (2002) 124.
[43] J.C. Light, J. Chem. Phys. 40 (1964) 3221.
[44] W.J. Chesnavich, M.T. Bowers, J. Am. Chem. Soc. 98 (1976) 8301.
[45] W.J. Chesnavich, M.T. Bowers, J. Chem. Phys. 66 (1977) 2306.
[46] J.C. Choe, B.J. Kim, M.S. Kim, Bull. Kor. Chem. Soc. 10 (1989) 167.
[47] V.H. Dibeler, R.M. Reese, M. Krauss, Adv. Mass Spectrom. 3 (1966) 471.
[48] A.G. Harrison, Chemical Ionization Mass Spectrometry, CRC Press, Boca Raton, FL, 1983.
[49] A. Sinha, M.C. Hsiao, F.F. Crim, J. Chem. Phys. 94 (1991) 4928.
[50] G.E. Busch, K.R. Wilson, J. Chem. Phys. 56 (1972) 3638.
[51] R. Lide, Handbook of Chemistry and Physics, 78th ed., CRC Press, Boca Raton, FL, 1997.